Zhao, X., Sun, J., Liu, S., Long, Z., Yin, Y., and Chen, Q. 2021. "Inverse design of the thermal environment in an airplane cockpit using the adjoint method with the momentum method," *Indoor Air*, 31:1614-1624.

Inverse design of the thermal environment in an airplane cockpit using the adjoint method with the momentum method

Xingwang Zhao[1, 2, 3], Jingnan Sun[2], Sumei Liu[2, 3], Zhengwei Long[2], Yonggao Yin[1, 4], Qingyan Chen[3,*]

[1]School of Energy and Environment, Southeast University, Nanjing 210096, China
[2]Tianjin Key Laboratory of Indoor Air Environmental Quality Control, School of Environmental Science and Engineering, Tianjin University, Tianjin 300072, China
[3]School of Mechanical Engineering, Purdue University, West Lafayette, IN 47907, USA
[4]Engineering Research Center of Building Equipment, Energy, and Environment, Ministry of Education, China

[*]Corresponding email: yanchen@purdue.edu

Abstract

Currently, the thermal environment in airplane cockpits is unsatisfactory and pilots often complain about a strong draft sensation in the cockpit. It is caused by the unreasonable air supply diffusers design. One of the best approaches to design a better cockpit environment is the adjoint method. The method can simultaneously and efficiently identify the number, size, location and shape of air supply inlets and the air supply parameters. However, the real air diffuser needed to design often have grilles, especially in the airplane cockpit, and the current method can only design the inlet as an opening. This study combined the adjoint method with the momentum method to directly identify the optimal air supply diffusers with grilles to create optimal thermal environment in an airplane cockpit (1) under ideal conditions and (2) with realistic constraints. Under the ideal conditions, the resulting design provides an optimal thermal environment for the cockpit, but it might not be feasible in practice. The design with realistic constraints provides acceptable thermal comfort in the cockpit, but it is not optimal. Thus, there is an engineering trade-off between design feasibility and optimization. All in all, the adjoint method with the momentum method can be effectively used to identify real air supply diffusers.

KEYWORDS: *Cockpit; Thermal environment; Inverse design; Environmental conditioning systems (ECS); Adjoint method; Momentum method*

Practical Implications

- The adjoint method with the momentum method can provide a much better design than current practice.
- The proposed method can be used to inversely design ideal indoor environment for buildings and transportation, such as airplanes, trains, cars, etc.

- Any reasonable demands for indoor environment, such as ideal indoor air quality, identification of contaminant sources, less energy consumption, etc, can be achieved using the adjoint method.

1 INTRODUCTION

According to the World Aviation Training Summit (2019 WATS) of the International Air Transport Association (IATA)[1], a total of 4.4 billion passengers travelled by airplane in 2018. The International Civil Aviation Organization (ICAO) has estimated that the number of global air passengers will reach six billion in 2030[2]. With the rapid growth in demand for air travel, the thermal environment in commercial airliner cabins and cockpits has attracted more and more attention. Currently, this environment is unsatisfactory, often being either too hot or too cold[3, 4]. Numerous studies[5, 6] have addressed the improvement of thermal comfort in passenger cabins, but few have focused on cockpits. The avionics in cockpits dissipate a large amount of heat, and cockpits are exposed to strong solar radiation through large windows. In order to remove the heat, a large volume of cold air is needed. Since a cockpit is a very small space, it is difficult to design air distribution without creating drafts for pilots. A questionnaire survey [4] found that cockpit drafts caused an inability to focus and fatigue on the part of pilots. In addition, the thermal environment in a cockpit can affect pilots' mental and physical health [7, 8]. It is important to create a healthy and thermally comfortable environment in cockpits, and the environmental conditioning system (ECS) of the airplane plays an important role. Therefore, it is crucial to design an optimal ECS for airplane cockpits. Traditional ECS design is based on the designer's individual experience and is thus a trial-and-error process, rarely capable of identifying the optimal solution. Recently, researchers have sought to use inverse design methods to improve thermal environments in buildings and passenger cabins[9]. The inverse design means that one is attempting to identify the unknown optimal boundary conditions based on the known information in the design domain subject to a set of constraints, such as the desired local velocity field. These include the genetic algorithm (GA)[10], the proper orthogonal decomposition (POD) method[11], the artificial neural network (ANN)[12], and the adjoint method[13].

The GA method[10] which is a stochastic search method can provide a globally optimal solution. However, when the number of design variables increases, the amount of calculation needed to find the global optimum will increase exponentially. To reduce calculation time, the POD method[11] simplifies the highly nonlinear relationship between the objective function and the design variables, using fewer samples. The ANN[12] aims to build a functional relationship between the objective function and the design variables through a limited number of samples. If the ANN is not well-trained by enough samples which contains all the characteristics of the problem, the prediction will introduce errors[14].

Unlike the three methods described above, the adjoint method[13] is a gradient-based optimization method. Liu and Chen[13] firstly introduced the adjoint method for inverse design of indoor environment. The adjoint method is adopted to calculate the gradient of the objective function and the optimization algorithm is used to update the design variables until the objective function achieve the optimal. It can find the optimal solution accurately and

efficiently, although an inappropriate initial state will cause the objective function to converge to a local optimum. In general, the adjoint method is the most suitable and promising method for the inverse design of a closed indoor environment. Liu et al.[15] developed an adjoint method with the use of the finite element method to design the size and location of inlets and the air supply parameters. However, it is very difficult to use this method to determine the optimal shape and number of inlets. An adjoint method with a filter-based topology method, proposed in our previous research [16, 17], has been successfully used to simultaneously design the number, size, location and shape of inlets and the air supply parameters for a laboratory-built environment, and has been validated experimentally. The present investigation adopted the adjoint method with the filter-based topology method to design an optimal thermal environment in an airplane cockpit. This paper discusses the inverse design process for the air supply system.

2 METHODS

2.1 Adjoint method

Our goal was to design a thermally comfortable environment in an airplane cockpit. In a similar manner to the use of indexes in the built indoor environment[17], this study employed the modified predicted mean vote for air cabins (PMVc)[18] index as shown in Eqs. (1) and (2) and the percent dissatisfied due to draft (PD) index[19, 20] as shown in Eqs. (7) for evaluating thermal comfort and draft sensation, respectively. The scale range of PMVc is the same with PMV which varies from -3 (cold) to 3 (hot). Zero means the neutral.

$$\mathrm{PMV_c(summer)} = -0.0758\mathrm{PMV}^2 + 0.6757\mathrm{PMV} - 0.1262 \tag{1}$$

$$\mathrm{PMV_c(winter)} = -0.0696\mathrm{PMV}^2 + 0.6906\mathrm{PMV} - 0.1369 \tag{2}$$

where

$$\begin{aligned}\mathrm{PMV} = {} & (0.303e^{-0.036M} + 0.028)\times\{(M-W) - 3.05\times10^{-3}\times[5733 - 6.99(M-W) - p_{\mathrm{amb}}] \\ & - 0.42\times[(M-W) - 58.15] - 1.7\times10^{-5}\times M\times(5867 - p_{\mathrm{amb}}) - 0.0014\times M\times(34-\mathrm{T}) \\ & - 3.96\times10^{-8} f_{cl}\times\left[(t_{cl}+273)^4 - (t_r+273)^4\right] - f_{cl}h_c(t_{cl}-\mathrm{T})\}\end{aligned} \tag{3}$$

$$\begin{aligned}t_{cl} = {} & 35.7 - 0.028(M-W) - I_{cl}\{3.96\times10^{-8}\times f_{cl}\times\left[(t_{cl}+273)^4 - (t_r+273)^4\right] \\ & + f_{cl}h_c(t_{cl}-\mathrm{T})\}\end{aligned} \tag{4}$$

$$h_c = \begin{cases} 2.38\times(t_{cl}-\mathrm{T})^{0.25} & 2.38\times(t_{cl}-\mathrm{T})^{0.25} > 12.1\sqrt{\mathrm{V}} \\ 12.1\sqrt{\mathrm{V}} & 2.38\times(t_{cl}-\mathrm{T})^{0.25} < 12.1\sqrt{\mathrm{V}} \end{cases} \tag{5}$$

$$f_{cl} = \begin{cases} 1.00 + 1.290I_{cl} & I_{cl} \le 0.078\,\mathrm{m^2\cdot{}^\circ C/W} \\ 1.05 + 0.645I_{cl} & I_{cl} > 0.078\,\mathrm{m^2\cdot{}^\circ C/W} \end{cases} \tag{6}$$

$$\mathrm{PD} = (34-\mathrm{T})(\mathrm{V}-0.05)^{0.62}(0.37\mathrm{VTu} + 3.14) \tag{7}$$

where M is the metabolic rate of human (W/m^2); W mechanical work done by the human (W); p_{amb} the water vapor pressure around the human (kPa); T air temperature; t_{cl} the temperature of the outer surface of the clothing (℃); f_{cl} the area factor of the clothing; t_r the mean radiation temperature (℃); h_c the convection heat transfer coefficient (W/(m^2·K)); I_{cl} the thermal resistance of clothing (clo); Tu the local turbulence intensity.

Since this study wanted to achieve two different targets evaluated by two different indexes at the same time, this investigation transformed the multi-objective problem into a single-objective design problem by the linear weighted sum method. The corresponding single-objective function is:

$$J(\xi) = w_1 \frac{\int_\Theta \frac{\left(PMV_c - PMV_{c,ideal}\right)^2}{PMV_{c,ref}^2} d\Theta}{\int_\Theta d\Theta} + w_2 \frac{\int_\Theta \frac{PD - PD_{ideal}}{PD_{ref}} d\Theta}{\int_\Theta d\Theta} \quad (8)$$

where ξ is the design variables vector; w_1 (0.455) and w_2 (0.545) which were the results of questionnaire[21] for built indoor environment are the weighting factors for the PMVc index and PD index, respectively; $PMV_{c,\,ideal}$ (0) and PD_{ideal} (0) are the ideal values for the predicted PMVc index and PD index, respectively; and Θ represents the design domain which is the enclose surface 0.1m away from the occupants. The reference values $PMV_{c,ref}$ and PD_{ref} used to normalize the PMVc and PD indexes, respectively, were 0.492 and 9.58. The best reference value for each index is the maximum magnitude value. But for some indexes, such as energy consumption, are difficult to get the maximum value. To demonstrate the universality of constructing the objective functions, this study selected the results of a reference case as shown in Figure 12(a) in discussion section. The weighting factors for the cockpit will be different from the values used in the building and there are no available values for the cockpit. In addition, this investigation was not focused on the determination of proper weighting factors for different indexes or the effect of weighting factors on inverse design results, so we directly applied the weighting factors in Zhao et al.[17, 21] as an example, to illustrate the construction of a single-objective function. The weighting factors can be changed to any reasonable values in future designs.

All state variables (air velocity **V** and temperature T) in the above single-objective function, as shown in Eq. (8), are constrained by Navier-Stokes equations. This study numerically solved RANS equations to obtain the air distribution in the cockpit and the RANS equations coupled with a turbulence model is the most suitable method for indoor engineering applications [22]. To minimize the above single-objective function as shown in Eq. (8), this study employed the adjoint method[23]. The adjoint method originated from the Lagrange multiplier optimization theory[24]. The Lagrange multiplier is used to solve the extremum problem constrained by nonlinear equations. Since it is very difficult and costly to directly solve the gradient of the objective function, the Lagrange multiplier method transforms the constrained extremum problem into an unconstrained extremum problem. By introducing a

new set of unknowns called the Lagrange multiplier (also known as the Lagrange multiplier, or adjoint variable), the constraint equations and the objective function are combined to build a new function, the Lagrange function. Then, the steepest decent method[25] was used to update the design variables ξ:

$$\xi_{n+1} = \xi_n - \lambda_n \frac{dJ}{d\xi_n} \tag{9}$$

where ξ_n, ξ_{n+1} are design variables of the current and subsequent design cycles, respectively; n is the design cycle; and λ_n is the adaptive step size in the current design cycle[26].

In order to determine the gradient of the objective function in Eq. (9), the adjoint method establishes an augmented objective function L, which transforms the constrained design problem into an unconstrained optimization problem by introducing a set of adjoint variables (p_a, $\mathbf{V}_a$, T_a, and $\nu_{t,a}$):

$$L = J + \int_\Omega \left(p_a, \mathbf{V_a}, T_a, \nu_{t,a}\right) \cdot \left(\mathbf{N}, \mathbf{R}\right) d\Omega \tag{10}$$

where Ω represents the fluid computational domain; p_a, $\mathbf{V}_a$, T_a, and $\nu_{t,a}$ are the adjoint pressure, adjoint velocity, adjoint temperature, and adjoint turbulent viscosity, respectively; and **R** represents the residual error of the turbulence model equations. When the numerical simulation is fully converged, the residual errors of the RANS equations **N** and turbulence model equations **R** are all equal to zero. Therefore, the augmented objective function L is actually equal to the objective function J. Solving the gradient of the objective function J transforms to solving the gradient of the augmented objective function L. This gradient can be obtained directly through the following chain rule:

$$\frac{dL}{d\xi} = \frac{\partial L}{\partial \xi} + \frac{\partial L}{\partial p}\frac{\partial p}{\partial \xi} + \frac{\partial L}{\partial \mathbf{V}}\frac{\partial \mathbf{V}}{\partial \xi} + \frac{\partial L}{\partial T}\frac{\partial T}{\partial \xi} + \frac{\partial L}{\partial \nu_t}\frac{\partial \nu_t}{\partial \xi} \tag{11}$$

Since the functional relationship between state variables and design variables is highly nonlinear and very complicated, it is difficult and costly to directly obtain the partial derivative of state variables. Therefore, the adjoint method sets the sum of the last four terms in Eq. (11) to zero:

$$\frac{\partial L}{\partial p}dp + \frac{\partial L}{\partial \mathbf{V}}d\mathbf{V} + \frac{\partial L}{\partial T}dT + \frac{\partial L}{\partial \nu_t}d\nu_t = 0 \tag{12}$$

Eq. (12) can be used to derive the adjoint equations of RANS equations coupled with a turbulence model. We then obtain the formula for the gradient of the augmented objective function:

$$\frac{dL}{d\xi}=\frac{\partial L}{\partial \xi}=\frac{\partial J}{\partial \xi}+\int_{\Omega}\left(p_a,\mathbf{V_a},T_a,\nu_{t,a}\right)\cdot\frac{\partial\left(\mathbf{N},\mathbf{R}\right)}{\partial\xi}d\Omega \tag{13}$$

Previous studies[23,27] only shows the continuous adjoint equations for the specific turbulence model. This study provides the general continuous adjoint equations derivation method of RANS equations with turbulent viscosity as shown in Eqs. (9)-(13). For the $\nu_{t,a}$ as shown in Eq. (13), the corresponding adjoint turbulence model used to solve $\nu_{t,a}$ can be derived by the selected suitable RANS turbulence models for a specific airflow category[28]. This study used RANS equations with the RNG k-ε turbulence model[6, 27-31] which is the most suitable model for predicting the cabin environment to predict the air distribution in a cockpit and calculate the objective function[32] during the inverse design process. Thus, the adjoint turbulent viscosity $\nu_{t,a}$ in Eq. (13) can be solved by the adjoint RNG k-ε turbulence model[23]. The corresponding adjoint equations of RANS equations coupled with the RNG k-ε turbulence model and the detailed formula for the gradient of the augmented objective function can be found in Zhao and Chen[23]. To simultaneously design the number, size, location and shape of inlets and the air supply parameters for an airplane cockpit environment; this study used the filter-based topology method, which the performance of the adjoint method[17].

2.2 Momentum method

Computational fluid dynamics (CFD) simulation requires setting reasonable boundary conditions to close the calculation domain, the air supply diffuser used to create the desired indoor thermal environment is one of the most important boundary conditions. However, the geometry of the real diffuser with grills is usually very complex. Modeling that real diffuser is possible, but it is not realistic to conduct the numerical simulation for the real diffuser. That is because the span between the fine size of the air diffuser and the dimensions of the indoor space that we are cared about is huge and directly conducting the numerical calculations is too time consuming.

Currently the adjoint method can only design the inlet as an opening, while the effective area used for supplying fresh air in the real scenario is smaller than the outline area of real inlet as shown in Figure 1(a). In addition, the available space for installing air supply diffusers with grilles in a cockpit is very small. Since meshing the real inlet, as shown in Figure 1(a), will make the model very complicated and increase the amount of calculation, this study adopted the momentum method[33, 34, 35] to simplify real inlet as an opening, as shown in Figure 1(b), which area is the same with real inlet. However, the opening with small velocity can only guarantee the correct mass flow rate m, as shown in Eq. (14), and the momentum of the supplied air is not correct. Therefore, this study added the momentum source term[35] $\mathbf{S}_\Phi$ lost by simplifying real inlet in the first layer cells, as shown in Eq. (15) and Figure 1(c), which are adjacent to the initial boundary. Figure 1(c) only shows the hexahedral mesh as an example; this method is also applicable to other types of grid very easily.

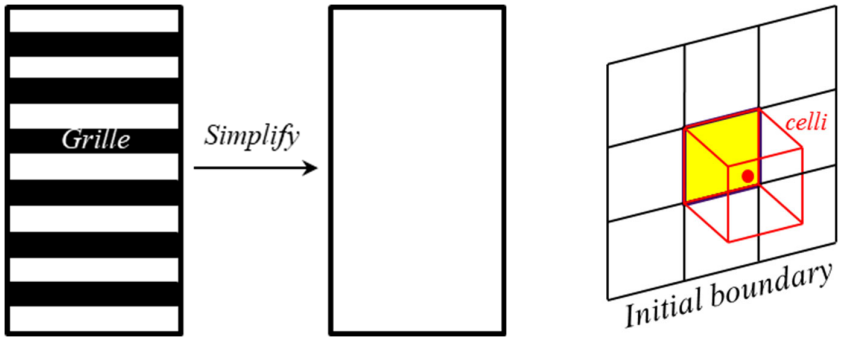

(a) (b) (c)

FIGURE 1 Simplification of the real inlet and the location used to apply the momentum source

$$m = \rho A_{inlet,eff} V_{inlet,eff} = \rho A_{inlet,geo} V_{inlet,geo} \quad (14)$$

The momentum source can be determined by:

$$\mathbf{S}_{\Phi} = m\mathbf{V}_{inlet,eff} - m\mathbf{V}_{inlet,geo} \quad (15)$$

where m is the mass flow rate; ρ the air density; $\mathbf{A}_{inlet,eff}$ and $\mathbf{V}_{inlet,eff}$ the effective area vector and the velocity of real inlet, respectively; $\mathbf{A}_{inlet,geo}$ and $\mathbf{V}_{inlet,geo}$ the area vector and the velocity of the simplified inlet, respectively.

2.3 Inverse design process

Figure 2 shows the flow chat of the inverse design process. For each specific problem, we firstly need to determine the locations of the potential optimal air supply inlets and initialize the air supply velocity ($\mathbf{V}_{inlet}$). With the application of the momentum method, the RANS equations coupled with a turbulence model were iteratively solved until the convergence was achieved. Then we checked whether the objective function achieved the convergence criteria. If not, the adjoint equations would be solved and the adjoint variables were used to calculate the gradient of the objective function. Finally, this study adopted the steepest decent method to update the design variables. The above process was repeated until the objective function reached the convergence criteria.

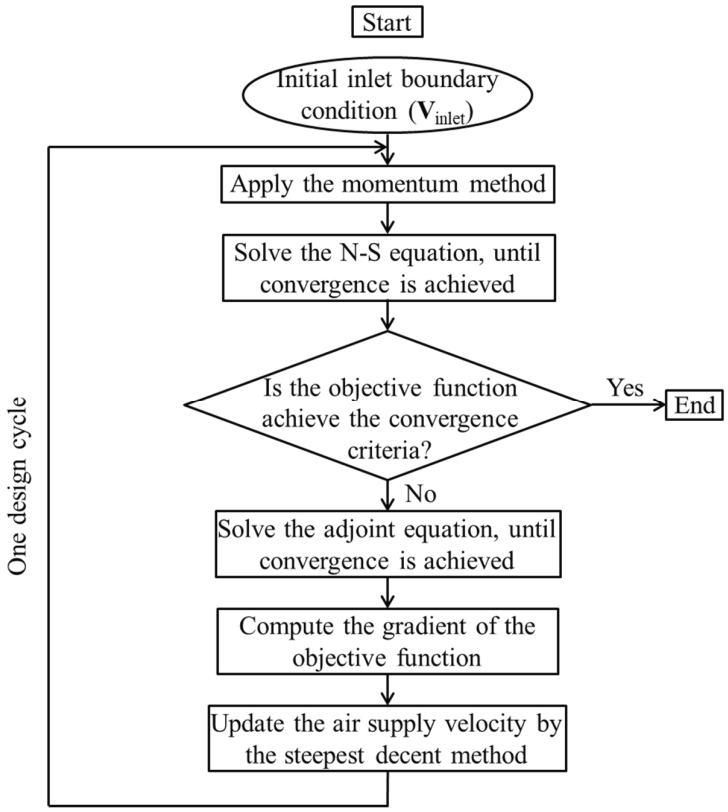

FIGURE 2 Flow chart of the inverse design process

The whole inverse design process employed in this investigation used the software implemented in Open Field Operation and Manipulation (OpenFOAM)[36]. To numerically solve the ordinary/adjoint continuity and momentum equations with an ordinary/adjoint turbulence model, the semi-implicit method for pressure-linked equations (SIMPLE) algorithm from Patankar and Spalding[37] was used to couple the ordinary/adjoint air velocity and air pressure. The convection and diffusion terms of the equations were numerically discretized by the first-order upwind scheme and the central difference scheme, respectively. This investigation also adopted the Boussinesq approximation[38] to simulate the buoyancy-driven flows in the non-isothermal indoor environment of the cockpit. The average y+ values used in this investigation was 3.05 and the standard wall functions was used for the near-wall treatment. Since the problems in real life are usually very complex and it is difficult to know whether the objective function is convex, the best solution is to find the optimal result under the set convergence criteria. The convergence criteria were set as $|J_n-J_{n-1}| < 0.01$ and the objective function no longer decreasing, where J_{n-1}, J_n were the objective function at the previous and current design cycles, respectively, and where $n \geq 2$. In our previous study, we have validated our CFD simulations ability using the experimental data[6]. So, this study conducted the CFD simulations directly.

2.4 Determination of the temperature boundary conditions in the cockpit

Figure 3(a) shows the cockpit geometry model used for the numerical simulation in this study. Different wall temperatures were set as the thermal boundary conditions. The temperatures of the heads and bodies of the pilots were 32ºC and 25ºC, respectively. These values were all obtained from thermal images captured in an actual airplane cockpit during flight, as shown in

Figure 3(b). Other boundary conditions, such as cabinets, seats, and consoles, were all set as adiabatic.

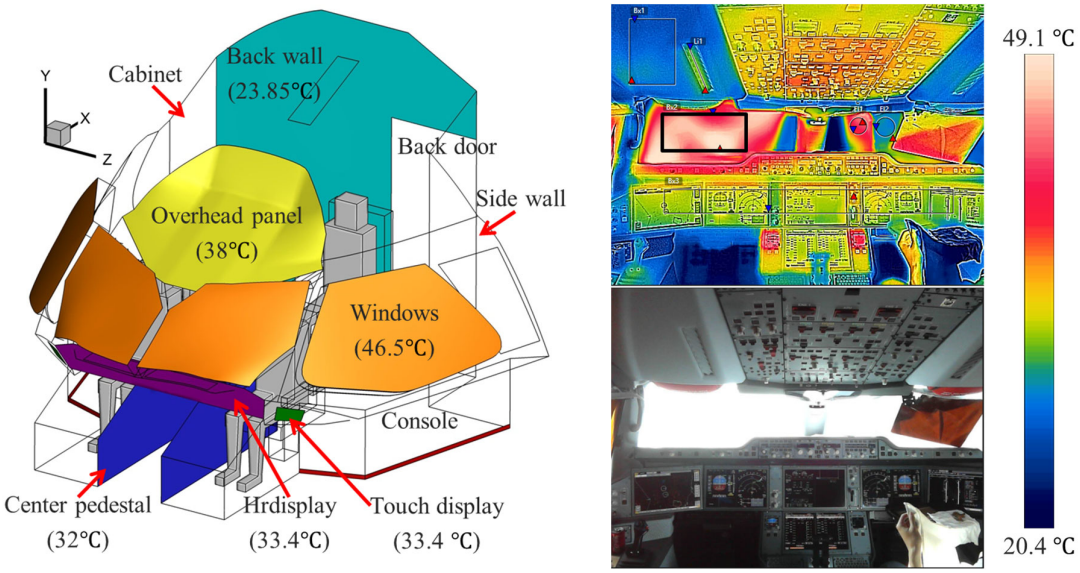

(a) (b)

FIGURE 3 (a) Surface temperatures and (b) thermal image of the cockpit

3 RESULTS

This section describes the detailed results obtained under ideal conditions and with realistic constraints.

3.1 Inverse design under ideal conditions

Traditionally, many parts of the cockpit could not be fitted with air supply diffusers. However, with the rapid development of technology, many previous design constraints are likely to be broken, the design under ideal conditions is to provide inspiration for the ideal design of the future. To achieve an optimal design, the preference would be to impose as few constraints as possible, which would occur under ideal conditions. Thus, unless there is equipment on a particular wall, that wall can be used as the location for thermo-fluid inlets. According to this reasoning, the green areas shown in Figure 4 were possible inlet locations for conditioned air: ceiling inlet (CI), left main inlet (LMI), left shoulder inlet (LSI), left front inlet (LFI), right main inlet (RMI), right shoulder inlet (RSI), right front inlet (RFI), floor inlet (FI), and back wall inlet (BWI). Since exhausts were not our design objective, this investigation simply specified the outlets in the side wall near the floor, as indicated by the red areas in Figure 4, according to experience [39, 40].

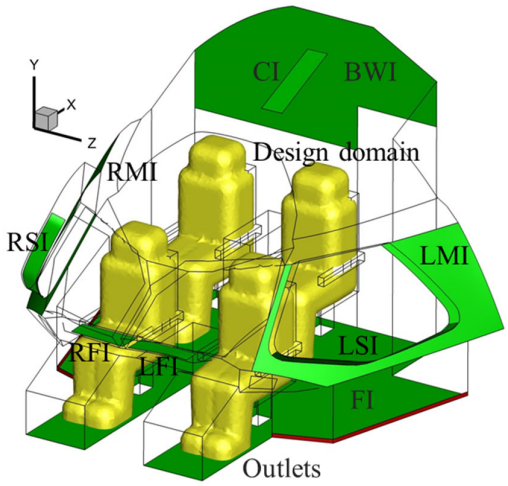

FIGURE 4 Initial air supply inlets, outlets and design domains Θ in the cockpit under ideal conditions

Our inverse design process under ideal conditions assumed a normal air supply velocity of 0.5 m/s and air supply temperature of 19ºC. Design variables were air supply velocity ($V_{inlet,x}$, $V_{inlet,y}$, and $V_{inlet,z}$) in cartesian coordinates and the direction of the air supply velocity can only be directed inside the cockpit. Our design objective was to minimize the objective function, J in Eq. (8), in the gold areas, which were the envelopes at a distance of 0.1 m from each pilot's body. Since this study employed the adjoint method, a grid-independence test was conducted, on the basis of which a mesh with 717,323 tetrahedral cells was selected (see further information in the discussion section). In addition, the total air flow rate was fixed at 0.17 m^3/s in accordance with the design cooling load.

Figure 5 illustrates the changes in the objective function J and air supply velocity distribution in the initial inlets during the inverse design process. The design variables were the number, size, location, and shape of the inlets and the air supply parameters. In each design cycle, we iteratively solved the RANS equations coupled with the RNG k-ε turbulence model and checked whether the objective function J met the convergence criteria. If not, we then solved the adjoint equations until the convergence criteria were achieved and employed the topology method[17] and the steepest decent method[25] to update the air supply velocity of each cell in all the initial inlets. As shown in the figure, the objective function did not change much between design cycle 10 and cycle 40. Compared with that in design cycle 1, the air supply velocity distribution in cycle 40 was much smaller.

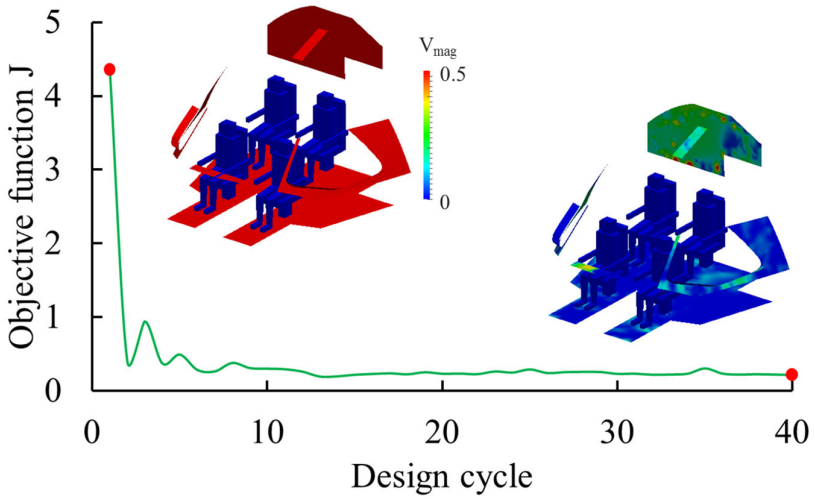

FIGURE 5 Changes in the objective function and air supply velocity distribution in the inlets under the ideal conditions

Figure 6 depicts in detail the air supply velocity distribution in the inlets at design cycle 40. Most of the flow should be supplied through inlets BWI (85%) and LMI (6.3%). The velocity in most areas of RMI, CI, and RFI was very high; however, the corresponding flow rates were only 3.6%, 2.6%, and 0.12% of the total air flow rate (0.17 m^3/s), respectively. Almost the entire BWI exhibited a velocity at the maximum (0.5 m/s), which indicates the main air supply. Note that, Figure 6 shows the three-dimensional velocity vector and the normal velocity of most part of BWI is very small.

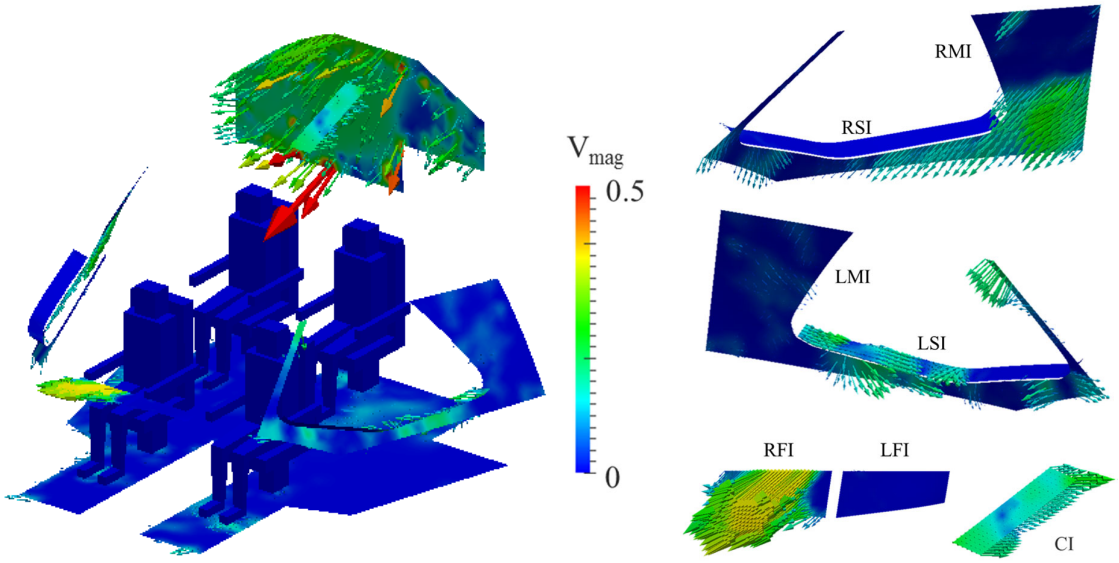

(a) (b)

FIGURE 6 Details of the air velocity distribution in the inlets under ideal conditions

Figure 7 shows the distributions of PMV_c and PD around the four pilots obtained by the

inverse design process. The PMV_c is close to zero (with an average of 0.28), and the PD is less than 10%. The inverse design can provide satisfactory results.

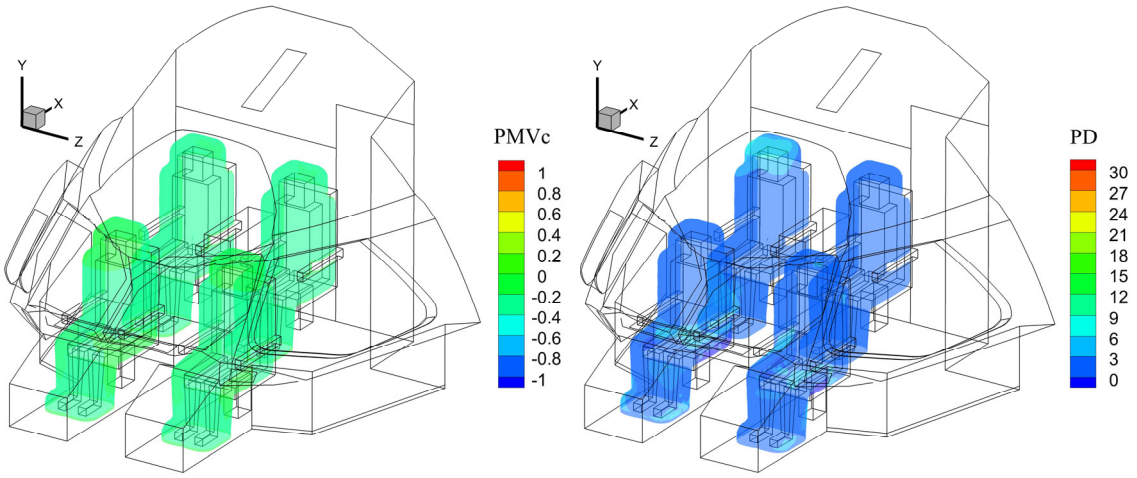

(a) (b)

FIGURE 7 Distribution of the design objectives around the pilots under ideal conditions: (a) PMVc (%) and (b) PD (%)

3.2 Inverse design under realistic constraints

Although the results of the inverse design process under ideal conditions look good, there are a number of constraints in reality. The constraints come from difficulties in manufacturing and from the need to compromise with other aircraft systems:

1) Many locations, such as the floor and back wall, should not have inlets.
2) Inlet size should be as small as possible.
3) The air supply temperature for the cockpit should always be the same as that for the passenger cabin.
4) The air supply velocity from an inlet should be uniform.
5) Almost all the inlets have grilles, and the effective area of an inlet is usually smaller than the outline of the inlet.

On the basis of the results obtained under ideal conditions and the above-mentioned realistic constraints, we closed both FI and BWI and reduced the sizes of LMI and RMI. Figure 8 shows the possible inlets with the realistic constraints. This investigation assumed an effective area ratio of 50% for all the inlets and used the momentum method [33,34,35] to simulate the inlets with grilles. Other settings remain unchanged from their state under ideal conditions.

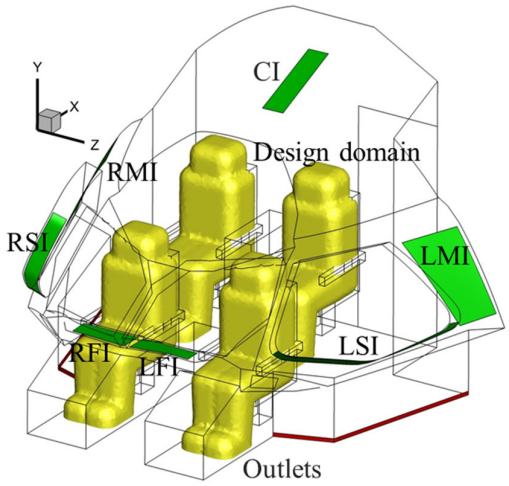

FIGURE 8 Initial air supply inlets in the cockpit with realistic constraints

Next, this investigation performed another inverse design. Figure 9 depicts the changes in the objective function J and air supply velocity distribution with the design cycle. The objective function J fluctuated in the first nine design cycles and then became relatively stable. The final objective function was equal to 0.27, which was slightly larger than the 0.21 achieved under ideal conditions. The reason why the objective function J of the final inverse design with many realistic constraints was close to the ideal objective function (0.21), was that the total airflow rate could vary. Figure 9 also shows the air supply velocity distribution at the first and final design cycles. Except for LMI and RMI, the velocities in parts or all of the other initial inlets were higher than 0.1 m/s. Thus, the optimal inlets would be in locations CI, LSI, LFI, RSI, and RFI.

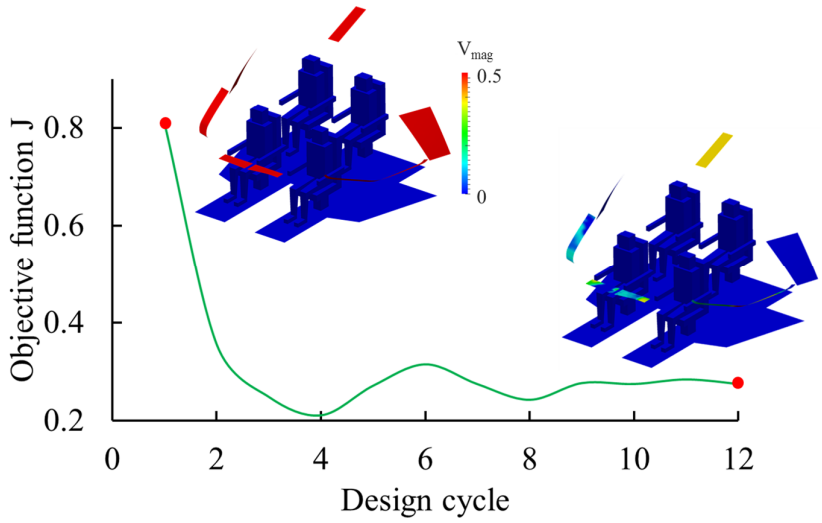

FIGURE 9 Changes in the objective function and air supply velocity distribution in initial inlets with the design cycle, with realistic constraints

Figure 10 depicts the area and flow rate for the inlets that were finally identified with realistic

constraints. The total flow rate for the final design was 0.1 m^3/s, which was equivalent to 17 ACH, and CI and LSI supplied 70% of the flow. The asymmetrical geometry of the cockpit was the direct cause the asymmetry of the inverse design results.

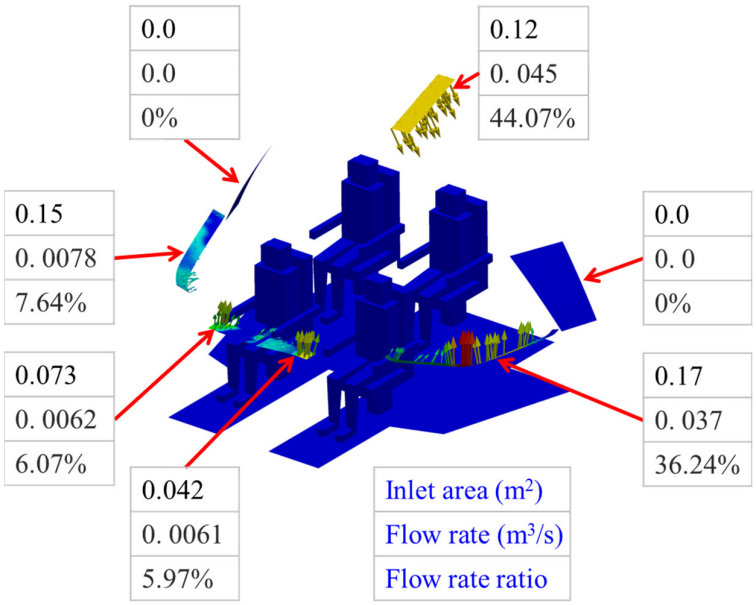

FIGURE 10 Area and flow rate for the inlets with realistic constraints

Figure 11 shows the PMVc and PD distributions around the pilots created by the above identified air supply inlets and parameters. The average of the absolute value of PMVc in the design domain was 0.3, as shown in Figure 11(a). Note that the PMVc and predicted mean vote (PMV) indexes are slightly different, but the recommended values are the same. The finally identified thermal comfort level, shown in Figure 11(a), satisfied the ISO7730 standard[41], which stipulates that the average $|PMV| < 0.5$. Similarly, the average PD (PD_{avg} = 1.6%) around the pilots (Figure 11(b)) also met the design standard in the ASHRAE Handbook[42], which recommends that the average PD be less than or equal to 15%. However, the PD around the upper body of the left front pilot was slightly higher. Compared with the results under ideal conditions, the results for this design were not ideal. This was because the final ECS was inversely identified under multiple realistic constraints, and the final results were the only ones that could be applied to a real airplane cockpit. In summary, the adjoint method can be used to design an optimal thermal environment in a cockpit, and the final design was a compromise between realistic and ideal.

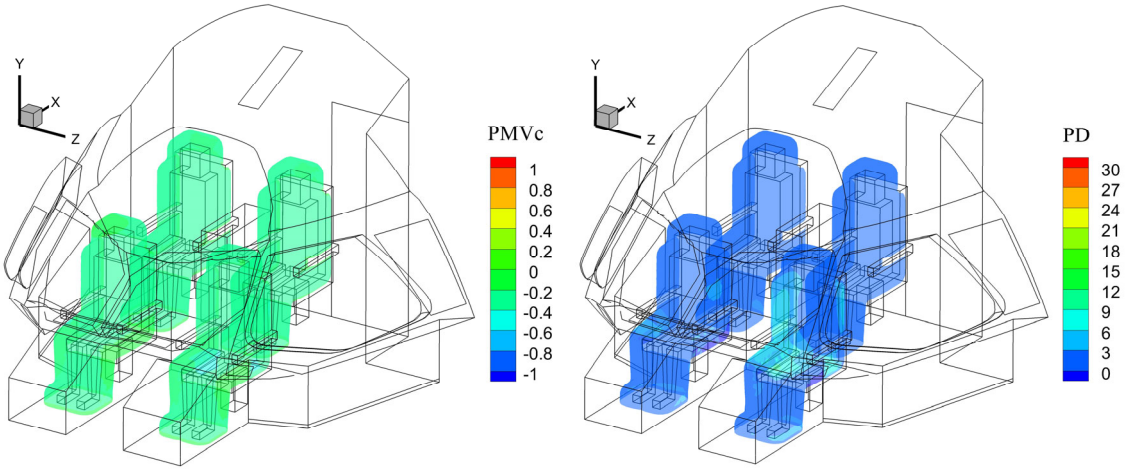

(a) PMVc distribution (b) PD distribution

FIGURE 11 PMVc (%) and PD (%) around the pilots with the final designed ECS at the 12th design cycle

4 DISCUSSION

Since we only have the new geometry of the cockpit model which will be used to the new airplane, we did not have the numerical results for the existing cockpits. To better quantify the new design results, this study introduced the PMVc and PD index to measure thermal comfort and draft sensation, respectively, in indoor environments. In addition, the PMVc index which was developed for passengers in aircraft cabins may not be suitable for the pilots. However, we did not find a better index to evaluate the pilots' thermal comfort. Future research would develop a more suitable index to evaluate the pilots' thermal comfort.

For that small and crowded cockpit, the locations of the outlet indeed influence the cockpit thermal environment. To decrease the effect of the exhaust air velocity, this study set the red areas away from the occupant zone, as shown in Figure 4, as the outlets. Future study can assume the outlet as the inlet with negative velocity to design the outlets using the same methods.

For ideal case, we know the total cold load and set the air supply temperature as a constant value. So, the flow rate should not be changed during the inverse design process. However, the cold load would change during the flight in the real scenario and the pilot would like to change the flow rate of the air supply inlets, that is one of the main reasons for setting different cases.

Figure 12(a) shows the reference cockpit used for grid-independence test. The green area and red area in that cockpit were the inlets' and outlets' potential locations respectively determined by traditional designers based on their experience. This investigation conducted a grid-independence evaluation using three different grid numbers: 0.16, 0.72, and 3.09 million tetrahedral cells. Figure 12(b) and (c) compare the velocity and temperature profiles with the three grid numbers, at the midpoint location among the four pilots. According to the results,

0.72 million cells were acceptable. Therefore, this investigation used a grid with 0.72 million cells for the inverse designs.

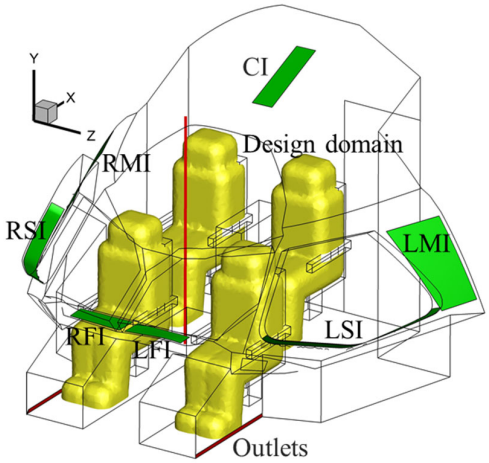

(a) Schematic of the reference cockpit

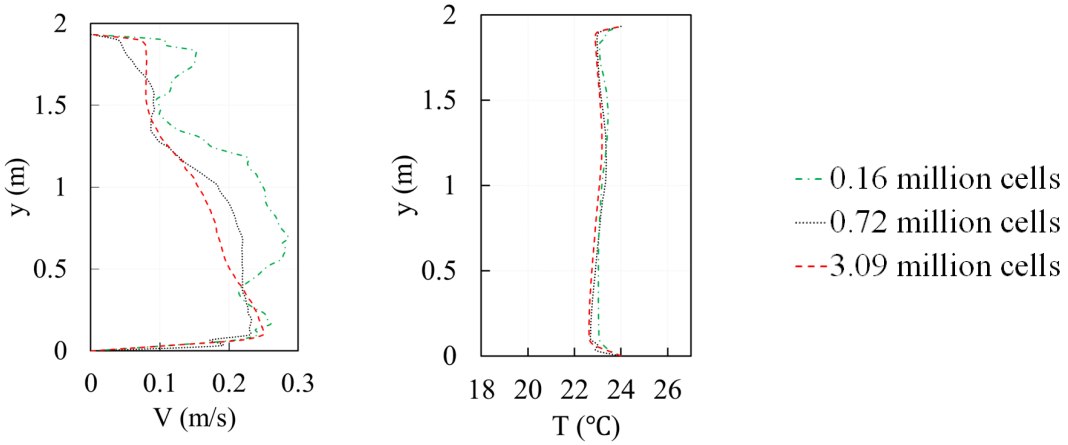

(b) Air velocity (c) Air temperature

FIGURE 12 Schematic of the reference cockpit (a) and comparison of (b) air velocity and (c) air temperature profiles at the midpoint among the four pilots with three different grid numbers

Since previous studies[5,16] could obtain reasonable results using the first-order upwind scheme to discretize the convection term of the ordinary/adjoint continuity and momentum equations with an ordinary/adjoint turbulence model, this investigation used the first-order upwind scheme directly. The effect of the high-order numerical scheme on the inverse design results is worth further exploration.

Note that the airflow rate used in the inverse design process under ideal conditions was fixed at 0.17 m^3/s, which was determined from the design cooling load. However, the flow rate for the final design under constrained conditions was a variable and could be reduced to 0.1 m^3/s. The design under ideal conditions could also use a variable airflow rate. Since the main

purpose of this study was to demonstrate the inverse design process for the cockpit, the difference in flow rates was not a major concern.

For real airplane cockpits, it would be impractical to manufacture air supply inlets that are as fragmented as those shown in Figure 6 and 10, with non-uniform air supply velocity. A designer could easily use the area constrained topology method and cluster analysis method[16, 17] to further consolidate the inlets if needed.

The benefit of the proposed method is that the inverse design process is automatic, and the identified results are optimal under the set convergence criteria. The result of section 3.2 has proved that the proposed method can design the optimal air supply diffusers to create a comfortable environment, even under the strict constrains. For the design in section 3.2, we only need 12 hours to finish the design. Note that, the CFD simulations in this study were conducted on a 20-core cluster with the Central Processing Unit (CPU) frequency of 2.60GHz for each core. While the trial-and-error method may need several mouths and try hundreds of times to finish the design which may also not be the optimal design.

5 CONCLUSIONS

This investigation demonstrated the inverse design of the thermal environment in a cockpit using the adjoint method with the momentum method. The following conclusions can be drawn:

- The adjoint method with the momentum method can be used to find real air supply inlet size and location and air supply parameters. The resulting design can significantly improve thermal comfort in a cockpit.
- The inverse design process under ideal conditions can find an optimal solution, although the resulting design may not be suitable for practical manufacturing. For this particular cockpit under ideal conditions, the proposed method can achieve that $\overline{|\mathrm{PMV}|}_{\Theta} = 0.28$, and $\overline{\mathrm{PD}}_{\Theta} = 1.2\%$.
- The inverse design process with realistic constraints can still provide a much better design than current practice, especially the draft sensation.
- The fewer of the constrains, the better of the results. Therefore, ideal design requires a certain degree of freedom.

REFERENCES

1. International Air Transport Association (IATA). World Aviation Training Summit (2019 WATS), Montréal, Canada; 2019.
2. International Civil Aviation Organization (ICAO). Annual Passenger Total Approaches 3 Billion According to ICAO 2012 Air Transport Results [Online]; 2012. Available from http://www.icao.int/Newsroom/Pages/annual-passenger-total-approaches-3-billion-according-to-ICAO-2012-air-transport-results.aspx (accessed January 2015).
3. Park S, Hellwig R T, Grün G, et al. Local and overall thermal comfort in an aircraft cabin and their interrelations[J]. Build Environ. 2011; 46(5): 1056-1064.
4. Johansson E. The thermal comfort of the cockpit: A pilot's experience[J]; 2017.
5. Liu W, Duan R, Chen C, et al. Inverse design of the thermal environment in an airliner

cabin by use of the CFD-based adjoint method[J]. Energy Build. 2015; 104: 147-155.
6. You R, Zhang Y, Zhao X, et al. An innovative personalized displacement ventilation system for airliner cabins[J]. Build Environ. 2018; 137: 41-50.
7. Nilsson E. One-Dimensional Human Thermoregulatory Model of Fighter Pilots in Cockpit Environments[J]. Division of Applied Thermodynamics & Fluid Mechanics. 2015; Department of Management and Engineering, Linköping. Hämtat från http://www.divaportal.org/smash/get/diva2:906798/FULLTEXT01.pdf.
8. Shetty J, Lawson C P, Shahneh A Z. Simulation for temperature control of a military aircraft cockpit to avoid pilot's thermal stress[J]. CEAS Aeronaut. J. 2015; 6(2): 319-333.
9. Chen Q, Zhai Z, You X, Zhang T. Inverse Design methods for Built Environment. Routledge, Oxford, England; 2017.
10. Zhai Z J, Xue Y, Chen Q. Inverse design methods for indoor ventilation systems using CFD-based multi-objective genetic algorithm[C]. Build Simul-China. 2014; 7(6): 661-669.
11. Wei Y, Zhang TT, Wang S. Prompt design of the air-supply opening size for a commercial airplane based on the proper orthogonal decomposition of flows. Build Environ. 2016; 96:131-141.
12. Zhang T, You X. A simulation-based inverse design of preset aircraft cabin environment. Build Environ. 2014; 82: 20-26.
13. Liu W, Chen Q. Optimal air distribution design in enclosed spaces using an adjoint method. Inverse Probl Sci Eng. 2015; 23(5): 760-779.
14. Zhang T, You X. Applying neural networks to solve the inverse problem of indoor environment. Indoor Built Environ. 2014; 23(8): 1187-1195.
15. Liu W, Jin M, Chen C, Chen Q. Optimization of air supply location, size, and parameters in enclosed environments using a computational fluid dynamics-based adjoint method[J]. J Build Perform Simul. 2016; 9(2): 149-161.
16. Zhao X, Liu W, Lai D, Chen Q. Optimal design of an indoor environment by the CFD-based adjoint method with area-constrained topology and cluster analysis. Build Environ. 2018; 138:171-180.
17. Zhao X, Shi Z, Chen Q. Inverse design of an indoor environment using a filter-based topology method with experimental verification[J]. Indoor air. 2020; 12661.
18. Cui W, Zhu Y. Systematic study on passengers' thermal comfort under low-airpressure environment in commercial aircraft cabin[C]. Annual Meeting of the Center for Cabin Air Reformative Environment, Chongqing, China; 2015.
19. FANGER P O, Christensen N K. Perception of draught in ventilated spaces[J]. Ergonomics. 1986; 29(2): 215-235.
20. Fanger P O, Melikov A K, Hanzawa H, et al. Turbulence and draft. The turbulence of airflow has a significant impact on the sensation of draft[J]. ASHRAE J. 1989; 31(4): 18-25.
21. Ncube M, Riffat S. Developing an indoor environment quality tool for assessment of mechanically ventilated office buildings in the UK-A preliminary study[J]. Build Environ. 2012; 53: 26-33.
22. Zhai Z J, Zhang Z, Zhang W, et al. Evaluation of various turbulence models in

predicting airflow and turbulence in enclosed environments by CFD: Part 1-Summary of prevalent turbulence models[J]. HVAC&R Res. 2007; 13(6): 853-870.
23. Zhao X, Chen Q. Inverse design of indoor environment using an adjoint RNG k-ε turbulence model[J]. Indoor air. 2019; 29(2): 320-330.
24. Allaire G. A review of adjoint methods for sensitivity analysis, uncertainty quantification and optimization in numerical codes. Ingénieurs de l'Automobile. 2015; 836:33-36.
25. Ortega BJM, Rheinboldt WC. Iterative solution of nonlinear equations in several variables. Chap. 8, Academic Press, New York; 1970.
26. Zhao X, Liu W, Liu S, et al. Inverse design of an indoor environment using a CFD-based adjoint method with the adaptive step size for adjusting the design parameters. Numer Heat Tr A-Appl. 2017; 71(7):707-720.
27. Papoutsis-Kiachagias EM, Zymaris AS, Kavvadias IS, et al. The continuous adjoint approach to the k-ε turbulence model for shape optimization and optimal active control of turbulent flows. Eng Optimiz. 2015; 47(3):370-389.
28. Zhang Z, Zhang W, Zhai ZJ, Chen QY. Evaluation of various turbulence models in predicting airflow and turbulence in enclosed environments by CFD: Part 2-Comparison with experimental data from literature. HVAC&R Res. 2007; 13 (6):871-886.
29. Yakhot V, Orszag S A, Thangam S, et al. Development of turbulence models for shear flows by a double expansion technique [J]. Phys Fluid Fluid Dynam. 1992; 4(7): 1510-1520.
30. Chen Q. Comparison of different k-ε models for indoor air flow computations. Numer Heat Tr B-Fund. 1995; 28:353-369.
31. Liu W , Wen J , Lin C H , et al. Evaluation of various categories of turbulence models for predicting air distribution in an airliner cabin. Building & Environment. 2013; 65:118-131.
32. Nielsen P V. Computational fluid dynamics and room air movement[J]. Indoor air. 2004; 14(7): 134-143.
33. Chen Q, Moser A. Simulation of a multiple-nozzle diffuser[C]. Proc. of 12th AIVC Conference. 1991; 2: 1-14.
34. Srebric J, Chen Q. Simplified numerical models for complex air supply diffusers[J]. HVAC&R Res. 2002; 8(3): 277-294.
35. Deng B, Wang J, Tang J, et al. Improvement of the momentum method as the diffuser boundary condition in CFD simulation of indoor airflow: Discretization viewpoint[J]. Build Environ. 2018; 141: 55-60.
36. OpenFOAM. The Open Source CFD Toolbox. http://www.openfoam.com, 2012.
37. Patankar S V, Spalding D B. A calculation procedure for heat, mass and momentum transfer in three-dimensional parabolic flows. Int. J. Heat Mass Transf. 1972; 15(10):1787-1806.
38. Boussinesq J. Theorie Analytique de la Chaleur, Gauthier-Villars; 1903.
39. GB50736-2012. Design Code for Heating Ventilation and Air Conditioning of Civil Buildings. Ministry of Housing and Urban-Rural Development, PRC, China; 2012.
40. Stein B. Building technology: mechanical and electrical systems[M]. John Wiley &

592 Sons; 1996.
593 41. ISO 7730. Ergonomics of the Thermal Environment - Analytical Determination and
594 Interpretation of Thermal Comfort Using Calculation of the PMV and PPD Indices
595 and Local Thermal Comfort Criteria, International Organization for Standardization;
596 2005: 7730.
597 42. ASHRAE. ASHRAE Handbook - HVAC Applications (SI). American Society of
598 Heating, Refrigerating and Air Conditioning Engineers, Atlanta; 2011.
599